Multi-scale modelling of silicon nanocrystal synthesis by Low Pressure Chemical Vapor Deposition.

Ilyes Zahi, Pierre Mur, Philippe Blaise, Alain Estève, Mehdi Djafari-Rouhani, Hugues Vergnes, Brigitte Caussat

Multi-scale modelling of silicon nanocrystal synthesis by Low Pressure Chemical Vapor Deposition

I. Zahi [a,b,c], P. Mur [b], Ph. Blaise [b], A. Estève [c], M. Djafari Rouhani [c], H. Vergnes [a], B. Caussat [a,*]

[a] LGC-ENSIACET/INPT, Université de Toulouse, 4 allée Emile Monso, BP 84234, 31104 Toulouse Cedex 4, France
[b] CEA-DRT-LETI-CEA-GRE, 17 Avenue des Martyrs, 38054 Grenoble Cedex 09, France
[c] LAAS-CNRS, Université de Toulouse, Avenue du Colonel Roche, 31077 Toulouse Cedex, France

A B S T R A C T

A multi-scale model has been developed in order to represent the nucleation and growth phenomena taking place during silicon nanocrystal (NC) synthesis on SiO_2 substrates by Low Pressure Chemical Vapor Deposition from pure silane SiH_4. Intrinsic sticking coefficients and H_2 desorption kinetic parameters were established by ab initio modelling for the first three stages of silicon chemisorption on SiO_2 sites, i.e. silanol Si—OH bonds and siloxane Si—O—Si bridges. This ab initio study has revealed that silane cannot directly chemisorb on SiO_2 sites, the first silicon chemisorption proceeds from homogeneously born unsaturated species like silylene SiH_2. These kinetic data were implemented into the Computational Fluid Dynamics Fluent code at the industrial reactor scale, by activating its system of surface site control in transient conditions. NC area densities and radii deduced from Fluent calculations were validated by comparison with experimental data. Information about the deposition mechanisms was then obtained. In particular, hydrogen desorption has been identified as the main limiting step of NC nucleation and growth, and the NC growth rate highly increases with run duration due to the autocatalytic nature of deposition.

Keywords:
Chemical vapour deposition
Silicon
Modelling
Density Functional Theory
Multi-scale approach
Nanocrystals

1. Introduction

It is becoming increasingly important to better understand the mechanisms involved during the initial stages of silicon film formation by LPCVD. This is due to the never-ending demand for higher integration in microelectronics, and to the unique physical properties of silicon nanocrystals (NCs) spontaneously formed during the initial stages of deposition on SiO_2 substrates when silane SiH_4 is used as the precursor [1,2]. These NCs present potential applications to form floating gates of flash memory structures. They have driven intensive research efforts because they are expected to show several advantages such as high program/erase speed, long data retention, low power consumption, etc. [3]. In order to reach such properties with a good reproducibility at an industrial scale, the NC area density and size distribution must be controlled as precisely as possible [3,4]. This constitutes a real challenge knowing that deposition durations do not exceed several tens of seconds on industrial loads of more than one hundred wafers of 8 in. in diameter in conventional hot wall LPCVD reactors [5]. Area densities of 10^{12} NCs/cm^2 corresponding to NCs of 5 nm in diameter spaced 5 nm apart are sought for optimal device performance [6,7]. Consequently, in order to ensure good deposition uniformities and reproducibility, it is mandatory to have a thorough understanding of the phenomena involved in the nucleation, growth and coalescence of NCs. This knowledge is also important for other applications of silicon NCs and for other deposition processes. For instance, silicon NCs produced by Plasma Enhanced CVD for the photovoltaic field involve the same nucleation and growth issues [8,9].

A lot of experimental information about silicon NC nucleation and growth is available in the literature. According to Leach et al. [10], mobile silicon adatoms are present during the deposition of silicon atoms on dielectric surfaces such as SiO_2. These adatoms are thought to accumulate and cluster to form stable nuclei that grow to cover the surface and eventually coalesce [11]. According to Nicotra et al. [7,12] who investigated Si NC formation using energy-filtered transmission electron microscopy: (i) NCs show a good wetting of the oxidised surface and their shape can be represented by a truncated sphere, and (ii) a continuous steady state of nucleation has been observed, i.e. the number of nucleation sites does not decrease markedly during NC deposition. For Kajikawa and Noda [11], CVD processes are characterised by the existence of an incubation period, within which (i) film deposition is slower than during continuous film growth and (ii) the deposition rate grows exponentially with time. This means that the deposited material enhances deposition as in an autocatalytic process. These authors state that the large differences in the sticking probability of CVD precursors can explain this incubation period, and also act on the mechanisms of NC nucleation and growth. Indeed, it is well known that for classical LPCVD conditions silane homogeneously decomposes into unsaturated molecules Si_nH_{2n} and polysilanes Si_nH_{2n+2}[13,14]. All these species can

* Corresponding author at: Laboratoire de Génie Chimique, ENSIACET/Institut National Polytechnique de Toulouse, 4 allée Emile Monso-BP84234, 31104 Toulouse Cedex 4, France. Tel.: +33 5 34 32 36 32; fax: +33 5 34 32 36 97.
E-mail address: Brigitte.Caussat@ensiacet.fr (B. Caussat).

contribute to silicon deposition. However, the sticking coefficient of all unsaturated species is most often assumed to be equal to one, whereas that of saturated molecules is at least several orders lower [15–17]. Thus, it is likely that these various silicon precursors contribute to both nucleation and growth phenomena differently during the first stages of Si film formation on SiO_2 substrates.

The outer surface of thermal silicon dioxide substrates is composed of siloxane Si—O—Si and silanol Si—OH bonds [18]. The respective proportions of each of these bonds on a given surface depend on the exact oxidation conditions, on substrate pre-treatment and on the thermal history of the substrate. Siloxane bonds are known to be more thermally stable and less reactive than silanol bonds [18]. Miyazaki et al. [19], Mazen [20] and Mazen et al. [6] have shown that the pre-treatment of SiO_2 surfaces with hydrofluoric acid (HF) increases the area density of silanol bonds and also proportionally that of silicon NCs synthesised by LPCVD, whereas the NC size decreases. The use of SiO_2 substrates with high Si—OH bond densities is then a key to reaching high NC densities useful for quantum devices [6,18].

Miyazaki et al. [19] measured activation energy for nucleation on HF pre-treated SiO_2 substrates as being half of that measured on non-treated surfaces. They explain this fact by the reaction of the unsaturated silylene SiH_2 on silanol bonds. Mazen et al. [6] also suggest that SiH_2 could play a major role in the nucleation and growth of NCs. However, these points have not been explicitly investigated and many determining elements remain unknown.

Numerous authors have developed numerical models of CVD reactors calculating silicon deposition rates from silane and the homogeneously born species for given operating conditions [15,21–23]. However, to date, none of these researchers has studied the first stages of deposition with the exception of a previous study by our group [24]. By comparing experimental and calculated NC deposition rates using the Computational Fluid Dynamics (CFD) code Fluent, it has been observed that the classical kinetic laws of the literature largely over-estimate deposition rates for these ultrathin layers. The reason for this is that the available kinetic laws are only valid for continuous silicon films of conventional thickness, i.e. at least several tens of nanometers thick. During the first stage of deposition, it is likely that the surface bonds present on SiO_2 substrates play a key role and that nucleation and growth phenomena are slower than on an ever-growing silicon layer.

Consequently, this work aims to establish valid kinetic data for the first stages of silicon deposition on SiO_2 substrates and furthermore to develop an original multi-scale model to analyse the nucleation and growth phenomena occurring during NC synthesis from silane. Intrinsic sticking coefficients characteristic of precursor/surface site interactions deduced from ab initio modelling will be first presented. These sticking coefficients were implemented into the CFD code Fluent at the industrial LPCVD reactor scale in transient conditions by activating the Fluent system of surface sites control. Some information on the multi-scale coupling will be given before presenting and discussing the results obtained. In particular, a comparison between experimental and calculated NCs densities and radii will be performed.

2. Experimental details

Silicon NCs were deposited from pure silane in an industrial tubular hot wall LPCVD reactor manufactured by Tokyo Electronic Limited (TEL), as previously detailed [5]. The Si wafers were all thermally oxidised in dry mode at 1123 K. Two kinds of SiO_2 substrate were studied: a "non-treated" and a "treated" one. The SiO_2 thickness for the "non-treated" substrate was 5 nm. Prior to deposition, standard ozone cleaning was performed. According to Mazen [20], dry oxidation mainly provides siloxane Si—O—Si surface bonds. For the treated substrates, a 7 nm thick dry silicon dioxide layer was grown and just before deposition, a thickness of 2 nm was etched off in a dilute (0.2%) aqueous HF solution in order to break the Si—O—Si bridges to form much more reactive silanol Si—OH bonds, as measured by Mazen [20].

Deposition in the central part of wafers was analysed by Field Effect Gun Scanning Electron Microscopy (FEG SEM) on a Hitachi S5000 microscope, and by spectroscopic ellipsometry on a KLA Tencor UV1280. NC area density was measured by direct counting on FEG SEM images. Average values were taken from three counts on surface views of 200 nm × 200 nm. Spectroscopic ellipsometry allowed for the determination of the equivalent thickness and the silicon fraction of a continuous layer including vacuum and silicon (Effective Medium Approximation model). The diameter D of the as-deposited NCs was calculated by assuming the NCs to be hemispherical and using the following equation:

$$\pi * D^3 / 12 = e_{Si} / d_{dot} \quad (1)$$

where e_{Si} is the equivalent thickness of silicon and d_{dot} is the NC density (in number of NCs/cm^2); the intrinsic error on NC density and radius measurements was about 20%. The total number of silicon atoms deposited was deduced from the equivalent thickness of silicon e_{Si} and from the silicon diamond structure and mesh parameter (5.43×10^{-10} m), leading to 5×10^{28} silicon atoms/m^3.

Table 1 provides the operating conditions of the experiments used for this study, from Cocheteau [5], Mazen [20] and from our own results [25]. The same TEL reactor was used for the three studies and all the deposition experiments were performed by the same team of operators at CEA/Leti. Total pressure values were fixed between 16 and 27 Pa and temperatures to 590–600 °C for run durations of maximum 20 s. Only a few runs amongst the many performed could be considered because under the conditions tested, coalescence occurred very frequently especially on "treated" substrates. This explains that a temporal evolution of NC density and radius was obtained only for run D10NT for which a beginning of coalescence probably occurred after 15 s. Only runs leading to non-coalesced NCs were retained. In order to analyse the reproducibility of NCs synthesis, run D12TR is strictly identical to run D12T.

The corresponding experimental NC area densities and radii are presented as a function of run duration in Fig. 1. Logically, the treated substrates (runs D11T, D12T and D12TR) lead to the highest NCs densities. They also correspond to the lowest NCs radii. When comparing results obtained for runs D12T and D12TR, the relative difference between the two NCs densities is 19% and 13% for radii. Thus, the reproducibility of NC synthesis does not exceed 20% under the tested conditions. When comparing runs D10NT and D12NT, performed under the same conditions except for the total pressure, the NC density is higher for run D10NT, corresponding to the highest pressure tested. This is in agreement with the assumption that unsaturated species exalt NC nucleation, since homogeneous reactions leading to unsaturated species formation are favoured at high pressure. This will be more deeply studied by modelling in the next sections.

3. Chemical scheme of deposition and corresponding kinetic laws

Silane pyrolysis starts from a temperature of 350 °C and leads to numerous homogeneous and heterogeneous chemical reactions [21]. A simplified kinetic model was used for the homogeneous phase and

Table 1
Operating conditions tested.

Run	Operating conditions				
	Temperature (°C)	Pressure (Pa)	Run duration (s)	Substrate	Reference
D10NT	600	26.6	5–10–15–20	Non-treated	Mazen [20]
D11T	590	16	15	Treated	Cocheteau [5]
D12T	600	16	7	Treated	Cocheteau [5]
D12NT	600	16	7	Non-treated	Zahi [25]
D12TR	600	16	7	Treated	Zahi [25]

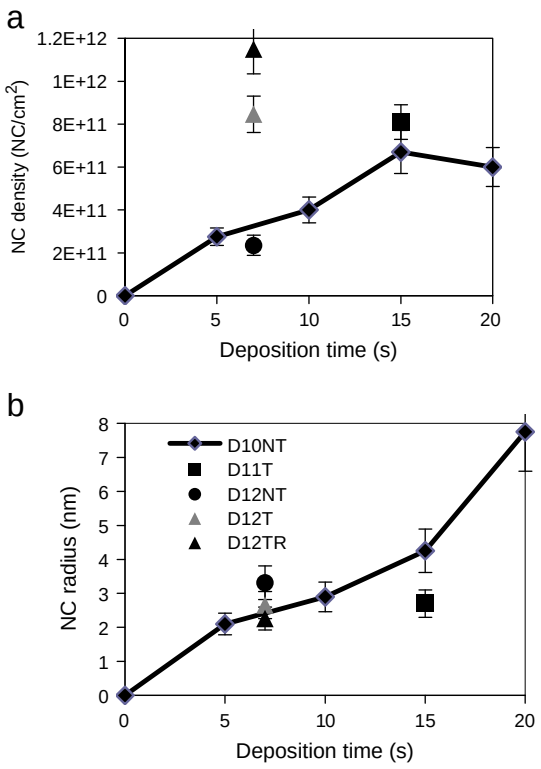

Fig. 1. Experimental NCs area densities and radii versus run duration.

two heterogeneous models, one valid for continuous thick silicon layers and the other specifically established by ab initio modelling for the first stages of silicon deposition on SiO_2 substrates.

3.1. Homogeneous reactions

The sole homogeneous chemical reaction considered is the formation of the unsaturated species silylene:

$$SiH_4 \leftrightarrow SiH_2 + H_2 (R_{hom})$$

The corresponding kinetic constants are those of Cordier et al. [17]. By considering only silane SiH_4 and silylene SiH_2 as silicon precursors, the kinetic scheme was purposely simplified regarding the number of species involved in silane pyrolysis to reach reasonable multi-scale simulation durations (minimum 3 days on a N-Series — Intel Core2 Quad Q6700). However, this choice does not limit the interest of the model because silylene is the main unsaturated species created in the gas phase. Moreover, it is also well known that the contribution to deposition of polysilanes of an order higher than 2 is negligible in LPCVD conditions [15,24].

3.2. Heterogeneous reactions in the case of thick Si layers

The two heterogeneous reactions considered are:

$$SiH_4 \rightarrow Si + 2H_2 (R_{het1})$$

$$SiH_2 \rightarrow Si + H_2 (R_{het2})$$

Following most previous studies found in the literature, a Langmuir–Hinshelwood formulation for silane decomposition onto surface using the kinetic constants of Wilke, Turner and Takoudis [26] was used. The kinetic theory of gases for silylene with a sticking coefficient of 1 was also applied [21].

3.3. Heterogeneous reactions in the case of NCs: ab initio results

As detailed in the introduction, conventional heterogeneous kinetic laws over-estimate deposition rates in the case of ultrathin Si layers [24]. Thus, it was necessary to establish new kinetic parameters by ab initio modelling to quantify interactions existing between SiO_2 surface bonds and precursor molecules and in particular to determine initial activation barriers and sticking coefficients.

As previously explained [27], interactions of SiH_2 and SiH_4 molecules on simple silanol Si—OH bonds, siloxane Si—O—Si bridged sites and fresh silicon bonds chemisorbed on SiO_2 surface have been analysed by DFT (Density Functional Theory). The reactions considered are schematically presented in Fig. 2 from chemisorption of the

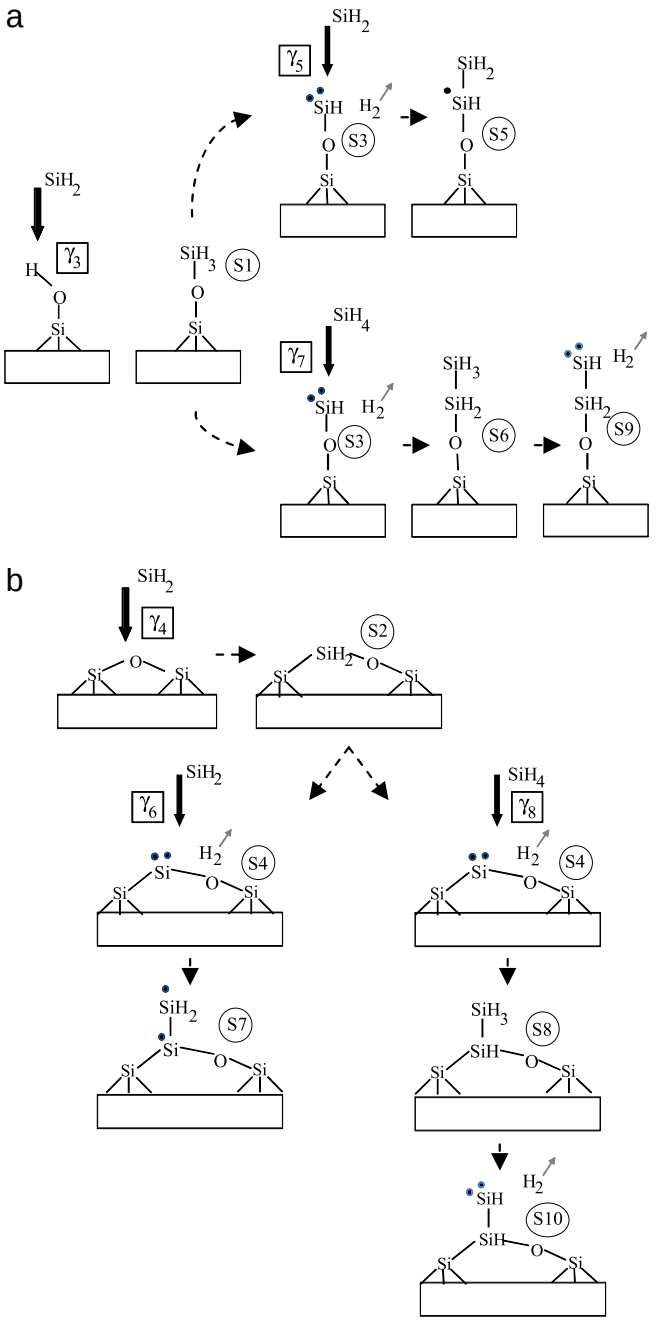

Fig. 2. Schematic representation of the chemical reactions and surface sites considered into Fluent during nucleation (a) on silanol sites, and (b) on siloxane bridges (*Si* into circles refers to the kind of surface sites).

Table 2
Sticking coefficients deduced from ab initio calculations.

Reaction	Precursor	Surface site	Sticking coefficient γ at 600 °C
1	SiH_4	Si—OH	$3.5 \cdot 10^{-18}$
2	SiH_4	Si—O—Si	$5.2 \cdot 10^{-18}$
3	SiH_2	Si—OH	0.0234
4	SiH_2	Si—O—Si	0.0017
5	SiH_2	S3	1
6	SiH_2	S4	1
7	SiH_4	S3	0.001
8	SiH_4	S4	0.01

precursor molecules on a SiO_2/Si based cluster ($Si_9O_5H_{12}$) up to the final structures considered.

The results obtained in terms of activation barriers, adsorption energies and formation energies indicating if the reaction is exothermic or endothermic, have already been presented and discussed [27]. Table 2 presents the sticking coefficients deduced using the methodology previously detailed [25]. They differ slightly from the results presented in [27] because of calculation refinements.

The sticking coefficients of silane on SiO_2 surface sites (reactions 1 and 2) are extremely weak indicating that silane cannot directly chemisorb on SiO_2. Consequently, these reactions were no longer considered and are not represented in Fig. 2. In contrast, SiH_2 sticking coefficients (reactions 3 and 4) are much higher, which means that the first silicon chemisorption on SiO_2 sites proceeds exclusively from unsaturated species like silylene. But, contrary to results in the literature for which the SiH_2 sticking coefficient is almost always supposed equal to 1 whatever the deposition surface, the present results show that the SiH_2 sticking coefficient is close to 10^{-2} on hydroxyl sites and to 10^{-3} on siloxane bridges. These new results agree with the experimental observations about a preferential nucleation of silicon on silanol bonds rather than on siloxane bridges. This can explain the existence of an incubation period for silicon NCs formation [11]. Silicon chemisorption from SiH_2 leads to new surface sites called S1 on silanol bonds and S2 on siloxanes bridges.

The second stage of silicon chemisorption needs the occurrences of hydrogen desorption from sites S1 and S2, leading respectively to sites S3 and S4. For Si chemisorption from SiH_2 (reactions 5 and 6), the SiH_2 sticking coefficient becomes equal to 1 on the two surface sites considered. Thus, for this species, the influence of the SiO_2 substrate disappears from the second stage of Si incorporation. For silane (reactions 7 and 8), the sticking coefficients are much higher than for the first stage, meaning that silane contributes to deposition by these reactions. It is worth noting that the SiH_4 sticking coefficient is ten times higher on S4 sites resulting from reaction 4 on siloxane bridges than on S3 sites resulting from reaction 3 on silanol bonds. This could be explained by the fact that the influence of oxygen is probably lower for S4 sites due to their Si—Si bond.

It should be noted that these silane sticking coefficients are higher than those deduced using classical kinetics. The global kinetics of Wilke et al. [26] for instance, leads to sticking coefficients close to 10^{-5} at 600 °C. However, these global sticking coefficients also include hydrogen desorption, which contributes to the slowing down of the whole scheme of silicon chemisorption as will be shown further. Thus, our DFT sticking coefficients considering only silicon chemisorption cannot be directly compared to the classical global ones.

Additional DFT simulations have been carried out to consider a third stage of silicon chemisorption. These results have shown that no sticking coefficient is modified in comparison with the second stage, confirming the disappearance of the SiO_2 substrate influence. Therefore, the first two steps of silicon chemisorption and all subsequent steps (on which the substrate has no more influence) are respectively termed 'nucleation' and 'growth' in the multi-scale model.

4. Model features

4.1. Fluent general features

Phenomena involved in the LPCVD process include tightly coupled fluid flow, heat transfer, mass transport of multiple gas species and chemical reactions in the gas phase and on surfaces of the reactive zone. Consequently, a numerical model for this process involves partial differential equations describing the conservation of mass, momentum, energy and chemical species associated with appropriate boundary conditions.

The reactor was simulated using the commercial CFD Fluent/Ansys® 12.1.4 software. Fluent is a pressure-based, implicit Reynolds Averaged Navier Stokes solver that employs a cell-centred finite volume scheme that has second-order spatial accuracy. This software discretizes any computational domain into elemental control volumes and permits the use of quadrilateral or hexahedral, triangular or tetrahedral and hybrid meshes.

Gas-flow and mass transfers including homogeneous and heterogeneous chemical reactions were calculated and the following assumptions were made:

- laminar gas flow (Re number lower than 10),
- ideal gas,
- due to its small surface area compared to the total silicon wafer area, the presence of the quartz wafer boat is ignored,
- the reactive zone is considered as axially symmetric, thus only a plane corresponding to a radius of the reactor has been studied,
- compressibility effects are not considered since the Mach number is at maximum equal to 0.1,
- reaction heats are ignored,
- the reactive zone and the gas phase are assumed to be isothermal, the temperature being fixed at the experimental one,
- simulations are performed in transient conditions to account for the temporal evolution of surface sites and of the precursors reactivity.

To develop this original multi-scale model without having overly long calculation times, only the entrance zone of the LPCVD reactor and the first thirteen wafers have been considered. A 2D geometrical domain of 2055 structured meshes was used to represent this zone. A sensitivity analysis of the grid size has been performed, showing that 2055 meshes offer a satisfactory precision.

The associated boundary conditions are the following:

- at the gas inlet, a flat profile is imposed on gas velocity; the total mass flux of species is fixed to the experimental one,
- at the exit, the total pressure is fixed to the experimental value,
- at the symmetry axis, classical Danckwerts conditions (derivatives equal to zero), are applied for all parameters,
- on the walls and wafer surfaces, a classical no-slip condition is used for gas velocity; the mass flux density of each species is assumed to be equal to the corresponding heterogeneous reaction rate.

The physical properties of the gaseous mixture were calculated from the Fluent data base. The simulation time step was fixed at 10^{-3} s after a sensitivity study of this parameter.

4.2. Multi-scale coupling

Two kinds of surfaces were considered. The first one corresponds to the reactor walls on which silicon had already been deposited. Then classical kinetic laws valid for thick silicon layers were applied.

The second kind of surface corresponds to wafers on which the DFT kinetics were applied. For these surfaces, the different sticking coefficients obtained by DFT (Table 2) were implemented into Fluent by activating its system of surface sites control in transient conditions [28]. Therefore, this multi-scale model needs to know the initial area density

of each type of SiO_2 surface site. This varies with temperature and chemical pre-treatments of the substrates.

4.2.1. Area density of SiO_2 sites

The operating temperatures for the present study are close to 600 °C. According to the valuable work of Vansant et al. [18], at this temperature, a SiO_2 surface is mainly constituted of isolated silanol or hydroxyl Si—OH sites and of siloxane Si—O—Si bridges. A low percentage (roughly 4%) of geminated silanol bonds has also been observed; for simplicity reasons, each geminated bond has been approximated by two simple silanol sites in our model.

According to [28–30], a completely hydroxylated SiO_2 surface corresponds to $4.6 \cdot 10^{18}$ sites/m^2, considering a cristobalite structure. This value has been retained as the total density of surface sites for the treated and untreated SiO_2 substrates.

For treated substrates, Vansant et al. have obtained $1.5 \cdot 10^{18}$ Si—OH sites/m^2 on SiO_2 at 600 °C. In this work the complementary value of $3.1 \cdot 10^{18}$ sites/m^2 has been attributed to siloxane bridges.

On the other hand, no information has been found in the literature concerning the number of Si—OH sites. Consequently, the results of Mazen [20] were used. These were obtained using the HMDS method. Indeed, the HMDS (hexamethyldisilazane) molecule decomposes in TMS (trimethylsilyl) groups exclusively on Si—OH sites. This author has measured a value of $0.55 \cdot 10^{18}$ Si—OH sites/m^2 on an untreated SiO_2 substrate annealed at 600 °C. Thus, it has been supposed that $0.55 \cdot 10^{18}$ Si—OH sites/m^2 and $4.05 \cdot 10^{18}$ Si—O—Si sites/m^2 were present on an untreated SiO_2 surface just before NCs synthesis at 600 °C.

4.2.2. Kinetic scheme of nucleation

In our multi-scale modelling NCs nucleation and growth steps are distinct but occur simultaneously. It must be re-stated that in this work nucleation concerns exclusively the first two stages of silicon chemisorption on either Si—OH or Si—O—Si sites and the first hydrogen desorption. Growth corresponds to subsequent stages of silicon chemisorption and hydrogen desorption.

The detailed kinetic scheme of nucleation has already been presented in Fig. 2. It is also important to remember that according to DFT results, only the unsaturated species SiH_2 can react on SiO_2 sites for the first silicon chemisorption.

The corresponding silicon deposition rate has been calculated by multiplying the deposition rate obtained from the kinetic theory of gases [21,31] (using our DFT sticking coefficients), by the surface coverage of the site on which the reaction occurs. It should be noted that the surface coverage corresponds to the ratio between the density of sites considered and the total surface sites density.

These first silicon chemisorptions from SiH_2 (reactions 3 and 4) lead to two new surface sites, respectively sites S1 and S2 in Fig. 2. Reactions of H_2 desorption have thus been considered, in order to create respectively the new chemisorption S3 and S4 sites. The kinetic law of hydrogen desorption has been calculated as follows:

$$V_{des-H2}(t) = \nu \times e^{-Ed/kT} \times \theta_{des-H2}(t) \times D_{total} \qquad \left(\text{kmol m}^{-2}\ \text{s}^{-1}\right) \tag{2}$$

E_d is the desorption energy deduced from our ab initio modelling [27]. D_{Total} corresponds to the total area density of surface sites which equals 7.64×10^{-9} kmol/m^2 (corresponding to $4.6 \cdot 10^{18}$ sites/m^2) and $\theta_{des-H_2}(t)$to the surface coverage of the desorption sites. No consensus exists in the literature on the value of the pre-exponential factor ν, representing the vibration frequency of the molecule. It is reported to vary between $10^{10}$and 10^{15} s^{-1}[32,33]. In testing this specific range of values, a major influence has been observed. It has been fixed at 7×10^{12} s^{-1} for all simulations performed, since this value provides the best fit with experiments. This is the only adjustable parameter of this multi-scale model.

The second chemisorption reactions correspond to reactions 5 and 6 from SiH_2 and reactions 7 and 8 from SiH_4. The corresponding kinetic laws are similar to those of the first silicon incorporations, considering the new surface coverage of sites on which the reaction occurs.

As illustrated in Fig. 2, a second hydrogen desorption step has been considered for sites S6 and S8, giving rise to sites S9 and S10 respectively. The kinetic law corresponds to Eq. (2).

S9 and S10 sites present molecular structures which are very similar to those of S5 and S7 sites. This DFT study [25] has shown that sites S5 and S7 are more stable than sites S9 and S10. Moreover, a nil value has been found for the energy barrier for H migration when simulating the hydrogen migration from a buried silicon atom to a surface one. Consequently, sites S9 and S10 have been considered as equivalent to sites S5 and S7 respectively. This has allowed for a 50% reduction in the possible mechanisms for the next steps and to also significantly shorten the Fluent calculation time.

Consequently, at the end of nucleation, the final molecular structures considered only correspond to S5 and S7 sites. It is clear that a lot of other configurations probably exist, their study is a perspective of the present work.

4.2.3. Transition between nucleation and growth

Both S5 and S7 sites present two dangling bonds, one on the buried silicon and the other on the surface silicon (Fig. 2). Therefore, these two silicon atoms are chemisorption sites for the next silicon incorporations steps. However, the Fluent system of surface site control assumes that the total number of surface sites is constant, one site continuously being replaced by another. This system does not allow for 3D growth such as that which occurs for silicon NCs. To bypass this limitation, a similar reactivity has been assumed for the two sites. The deposition rate of sites S5 and S7 has then been multiplied by two to consider the possibility of silicon chemisorption both on the buried and on the surface silicon atoms. Another step of hydrogen desorption has then been considered, always using Eq. (2).

4.2.4. Kinetic scheme of growth

Following the results of Nicotra et al. [7], NCs have been considered to be hemispherical. This form clearly implies a 3D growth, i.e. a growth in all spatial directions and not just vertically. Since the Fluent system of surface sites control cannot consider 3D growth, it has been assumed that each new chemisorbed silicon atom offers two dangling bonds of similar reactivity to gaseous precursors. The procedure from the previous section has thus also been applied. The results of Nicotra et al. [7], who found that critical NCs have a radius close to 1 nm, have also been used to calculate the area density of NCs. The contact surface between each critical NC and the substrate is then 3.6×10^{-18} m^2. Knowing that the number of silicon atoms per unit surface area is equal to 7×10^{18} atoms/m^2, the number of silicon atoms present between a critical NC and the substrate is therefore equal to 25.

The number of silicon atoms chemisorbed on substrate sites is calculated from the difference between the initial and current Si—OH and Si—O—Si surface coverages. The area density of NCs is thus equal to this number divided by 25.

The surface on which growth occurs corresponds to the outer surface of all the ever formed NCs. From Fluent results, it is easy to calculate the total number of silicon atoms deposited. Combining this result and the NC area density allows the NCs mean radius to be obtained, knowing that in this first version of the model, all NCs have been assumed to have the same radius. Consequently, the number of silicon atoms present on the whole NCs outer surface can be obtained from the corresponding hemispherical surface using the silicon mesh parameters.

It is worth noting that the number of silicon sites available for silicon chemisorption correspond to those for which H_2 desorption has already occurred. To account for them, a systematic counting of Si

growth sites before and after H_2 desorption has been performed by considering the hydrogen desorption rate for each kind of site.

It should be noted that the present version of the model does not consider any coalescence phenomenon, i.e. it has been assumed that nucleation may occur throughout the duration of deposition, as stated by Nicotra et al.

5. Results and discussion

5.1. Comparison between experiments and modelling

The comparison between the calculated and experimental NC densities temporal evolution is provided in Fig. 3. The calculated results tend to agree with the experimental ones. The error between simulations and experiments (reproducibility and NCs counting) is in the range of the experimental errors, i.e. close to 20%.

For run D10NT, from 5 to 20 s, only 1.4 to 2.5% of the initial substrate sites are covered. Such low values have also been obtained for the other runs. These results may be explained by the strong limitation of deposition imposed by the non-contribution of silane, by the relatively low silylene sticking coefficient and by its very low concentration. This result is in agreement with Nicotra et al. results. It should be noted that silane conversion does not exceed a few percent for all conditions tested and that the maximal SiH_2 mass fraction is 10^{-5}. Thus, the gas phase is mainly constituted of silane and of a small percentage of hydrogen during NCs synthesis. The simulation results show that the Si—OH sites are much more active for nucleation than the siloxane ones due to the higher SiH_2 sticking coefficient on silanol bonds.

The comparison between the calculated and experimental temporal evolutions of the total amount of silicon deposited per unit surface area is presented in Fig. 4. Again, it can be observed that the simulation follows the experimental trends, especially for run D10NT between 5 and 15 s and for runs D12T and D12TR. More important differences exist between experimental and simulated data for runs D11T and D12NT. It must be cited that the experimental total number of silicon atoms deposited has been deduced from equivalent continuous silicon thicknesses obtained by spectroscopic ellipsometry. Some differences have been noticed by Zahi [25] and Cocheteau et al. [5] between NCs radii measured by FEG SEM and those deduced from spectroscopic ellipsometry. This reveals some limitations in the precision of experimental results. Moreover, the difference specifically observed at 20 s for run D10NT could be explained by the non-consideration of coalescence by the model.

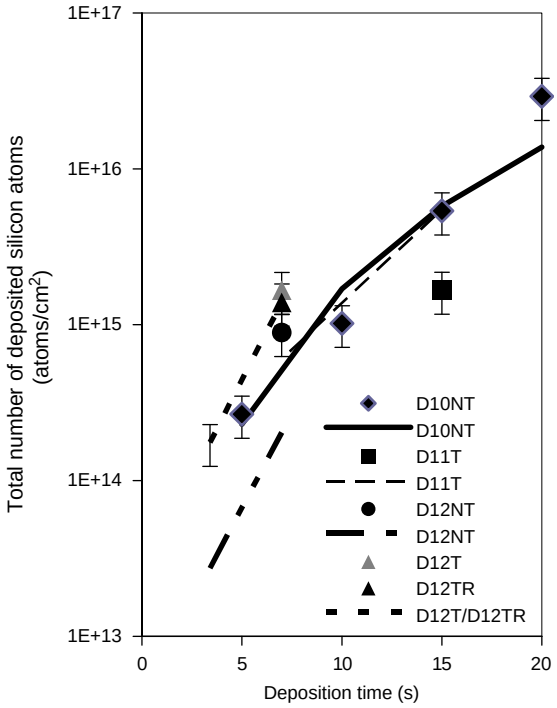

Fig. 4. Temporal evolutions of experimental (dots) and calculated (lines) total numbers of deposited silicon atoms.

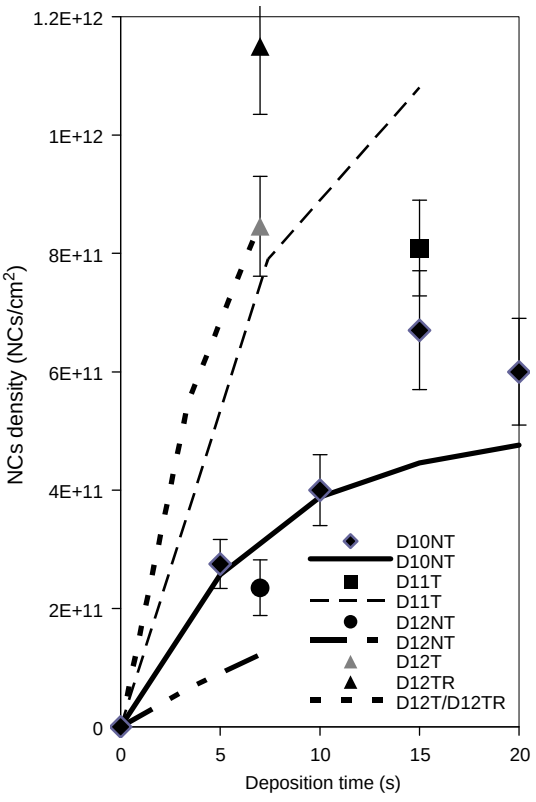

Fig. 3. Temporal evolutions of experimental (dots) and calculated (lines) NCs densities.

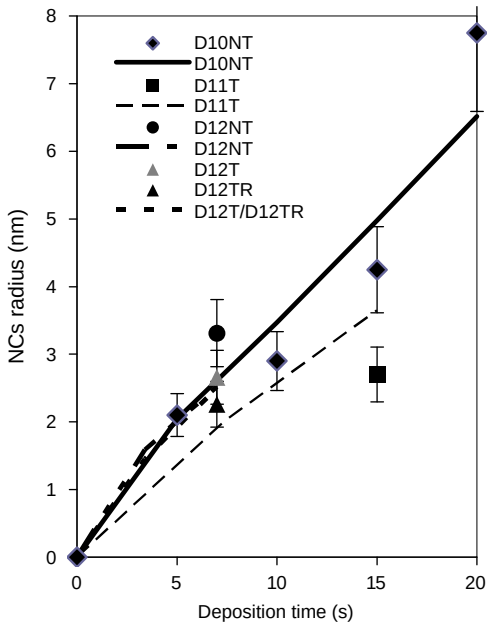

Fig. 5. Temporal evolutions of experimental (dots) and calculated (lines) NCs radii.

Fig. 5 presents the comparison between experimental and simulated NCs radii temporal evolution for the whole runs. For runs D10NT between 5 and 15 s and for run D12T, the difference between experimental and simulated results is lower than the experimental error. For run D10NT at 20 s, the underestimation of the radius by the model is again probably due to the non-consideration of coalescence.

To conclude, this comparison with experiments shows that considering the experimental errors, this first version of the multi-scale model provides a convenient representation of the NCs nucleation and growth for the operating range tested provided that coalescence is not reached.

5.2. Temporal evolution of some key parameters

The multi-scale model is now validated with the restrictions previously detailed. An analysis of the exact role of silylene and silane for Si nucleation and growth will be performed. The limiting steps of the NCs deposition process will also be outlined.

Fig. 6 presents the nucleation rate from silylene for the whole runs, Fig. 6(a) corresponds to the first silicon chemisorption (reactions 3 and 4 of Fig. 2) and Fig. 6(b) to the second one (reactions 5 and 6 respectively on sites S3 and S4, i.e. after the first hydrogen desorption). It appears that the first chemisorption step is clearly dominating, the second one being negligible. To explain this, it is worth noting that the first hydrogen desorption rate is very low (about 10^{-15} kmol m^{-2} s^{-1} equivalent to 8.5 10^{-6} Å/min) and that there is a factor 10^6 between site surface coverages just before and after this desorption. Thus the limiting step of nucleation is clearly H_2 desorption. For all runs, Fig. 6(a) indicates that the nucleation rate from silylene decreases with run duration because of the decrease of SiH_2 concentration in the reactor (not shown). This is due to the fact that the SiH_2 sticking coefficient is much higher for growth and therefore its contribution to growth increases with run duration. The highest nucleation rate is observed for run D10NT, corresponding to the highest temperature and pressure tested. Run D12T corresponds to the same temperature (600 °C) but to a lower pressure. It is then logical that the nucleation rate is lower since SiH_2 is formed in the homogeneous phase for which reactions are very sensitive to pressure. The nucleation rate is higher for run D12T than for run D12NT but only for the first second of deposition. This can be explained by the fact that the SiH_2 sticking coefficient is higher on Si—OH sites than on Si—O—Si ones, thus generating a higher initial nucleation rate. More growth sites are then created, leading to a higher consumption of silylene for growth to the detriment of nucleation as previously mentioned. It must be remembered that NC nucleation exists throughout run duration in this model.

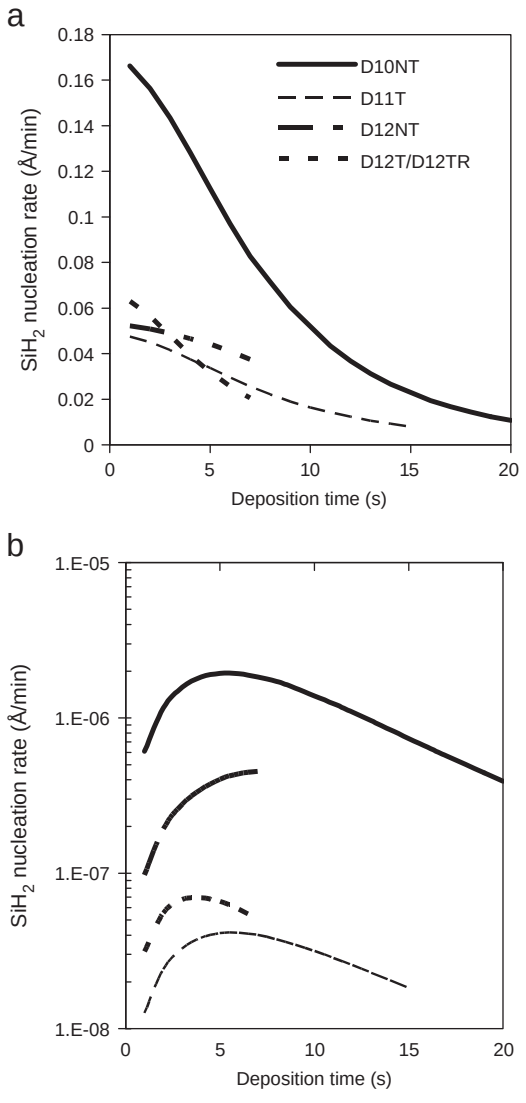

Fig. 6. Temporal evolution of the calculated SiH_2 nucleation rate: (a) first Si chemisorption, and (b) second Si chemisorption.

The nucleation rate from silane is presented in Fig. 7. This rate corresponds to silicon chemisorption from reactions 7 and 8 respectively on sites S3 and S4 born from the first silylene incorporation and from the first H_2 desorption. Notably, the rate increases with run duration because (i) the number of sites allowing this chemisorption increases with time and (ii) the silane concentration remains stable throughout deposition since very little is consumed during the reactions. The highest nucleation rate is again observed for run D10NT. When comparing runs D11T and D12NT, temperature appears to be a more influential parameter than substrate pre-treatments for these reactions. The nucleation rate from silane is higher for run D12NT than for run D12T because siloxane bridges are more numerous on non-treated substrates and the sticking coefficient γ_8 on sites S4 (born on siloxane bridges) is ten times higher than γ_7 on sites S3 (born on silanol bonds).

When comparing Figs. 6 and 7, it appears that silylene and in particular the first silicon chemisorption, is the main contributor to nucleation. This is certainly due to the marked difference between sticking coefficients of silane and silylene for nucleation. Another notable point is that under the conditions tested, the nucleation rates

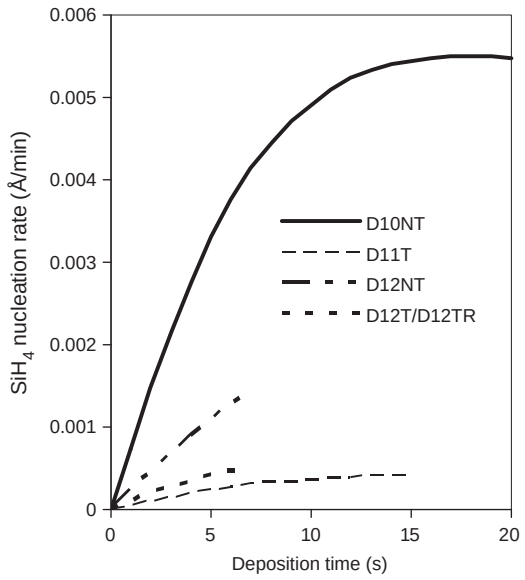

Fig. 7. Temporal evolution of the calculated SiH_4 nucleation rate.

from silane and silylene are very low since they never exceed 0.2 Å/min. This is due to the small concentration of the main contributor silylene.

Fig. 8 presents the growth rate from silylene. For the whole runs, this rate increases with run duration except after 15 s for run D10NT. However, as previously stated, the validity of results is no longer ascertained after run durations corresponding to the beginning of coalescence. This is clearly the case for run D10NT, after 15 s. Therefore, except for this point, the increase of growth rate from silylene with run duration is logical since the NCs surface and then the number of growth sites increase. In agreement with experimental observations, the highest growth rate is observed for the highest temperature (runs D11T and D12T) and for a same temperature (runs D10NT and D12NT), the highest value is obtained for the highest pressure tested leading to the highest SiH_2 concentrations. The substrate pre-treatment increases the growth rate from SiH_2 (runs D12NT and D12T), certainly because the NCs density and then the number of growth sites are higher.

Fig. 9 presents the growth rate from silane for the whole runs. For the same reason as for the SiH_2 growth contribution, this rate increases with run duration. In contrast to what has been observed for the other results, at this stage the substrate treatment has a pre-eminent influence. Indeed, though temperature and pressure for run D10NT are higher, results are similar for runs D10NT and D11T. The lower temperature and pressure for run D11T are compensated for by the higher number of growth sites due to the substrate pre-treatment. When comparing results obtained on substrates having undergone the same pre-treatment, an increase in growth rate from silane with temperature and pressure is logically observed. For the whole runs, results show a high increase in this rate with run duration t. This is in agreement with the simulation results of Cocheteau et al. [24] and with numerous experimental results indicating the existence of an incubation period and an autocatalytic behaviour of the deposition [11]. To better understand the origin of this evolution, we have calculated that the growth rate increases following a $t^{2.5}$ law, meaning that this increase is due to geometrical effects. Indeed, if it proceeds from a rising of the deposition area, the growth rate should increase as t^2 since the NCs radius evolution is linear versus time (Fig. 5) and the deposition area would be proportional to the square radius if NCs densities were constant. As NCs densities increase less and less with run duration (Fig. 3), the increase in the growth rate cannot be higher than a cubic law, which has been verified.

When comparing Figs. 8 and 9, the silylene contribution to growth is extremely low because of its very low concentration in the reactor. This logically corresponds to a classical result observed for LPCVD thick silicon layers [24].

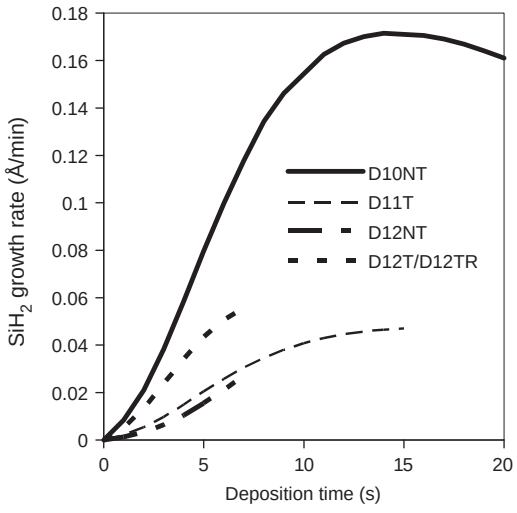

Fig. 8. Temporal evolution of the calculated SiH_2 growth rate.

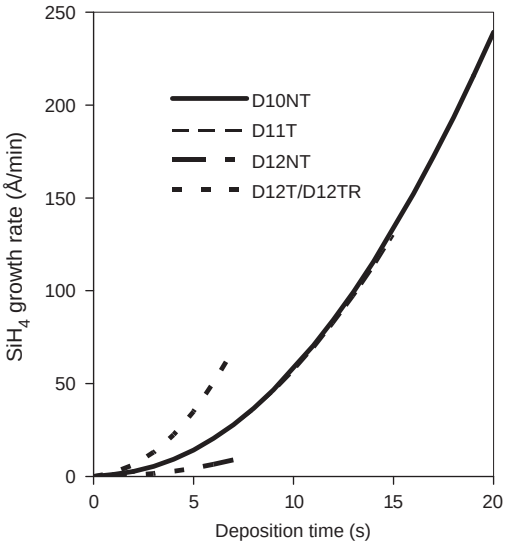

Fig. 9. Temporal evolution of the calculated SiH_4 growth rate.

Finally, when analysing the various sites surface coverage, factor 500 is observed between sites just before and after the second hydrogen desorption and factor 100 is seen for the third H_2 desorption. The second hydrogen desorption rate is as low as the first one previously commented. This hydrogen desorption is clearly the limiting step of growth.

6. Conclusion

A multi-scale model representing Si nanocrystals (NCs) nucleation and growth when synthesised by LPCVD from silane on SiO_2 substrates has been developed.

Ab initio calculations using DFT (Density Functional Theory) allowed to deduce sticking coefficients for the first silicon chemisorptions from silane and silylene and activation barriers for the first hydrogen desorptions on silanol Si—OH and silaxone Si—O—Si sites. Importantly, silylene has been found to be solely responsible for the first silicon chemisorption due to the fact that silane cannot chemisorb directly on SiO_2 sites. Furthermore, the silylene sticking coefficient for the first chemisorption is only 10^{-2} on silanol sites and 10^{-3} on siloxane ones. As reported in the literature, the silylene sticking coefficient for the second and subsequent silicon chemisorptions becomes equal to 1.

These DFT results were then implemented into the CFD code Fluent at the industrial LPCVD reactor scale in transient conditions by activating its system of surface site control. This multi-scale model was validated by comparison with experimental NC densities and radii synthesised at 590–600 °C between 16 and 27 Pa on treated and non-treated SiO_2 substrates for run durations not exceeding 20 s.

The analysis of the detailed phenomena involved during nucleation (i.e. the first two steps of Si chemisorption in this approach) revealed that the first H_2 desorption is the primary limiting step and that the nucleation rate is low (<0.2 Å/min) due to the very low concentration of silylene, which is the main contributor to the first Si chemisorption. Silane is the main contributor of growth (i.e. the subsequent Si chemisorptions), for which the limiting step is also hydrogen desorption. The growth rate highly increases with run duration due to the full autocatalytic character of the deposition process. It is now clear that homogeneously born unsaturated species like silylene should be favoured to enhance NC nucleation.

The multi-scale model has also provided original fundamental information about the early stages of silicon chemisorption on SiO_2 substrates. One of its major advantages is that ab initio results can be compared with experimental data. Ideas to improve the potentialities

of the model could include implementing coalescence criteria and using meso-scale modelling approaches like Monte-Carlo ones to better represent growth phenomena.

Acknowledgements

This work has been carried out in the framework of CEA/LETI/CPMA collaboration with PLATO organisation teams and tools.

References

[1] K. Makihara, H. Deki, H. Murakami, S. Higashi, S. Miyazaki, Appl. Surf. Sci. 244 (2005) 75.
[2] R.A. Puglisi, S. Lombardo, D. Corso, I. Crupi, G. Nicotra, L. Perniola, B. de Salvo, C. Gerardi, J. Appl. Phys. 100 (2006) 086104.
[3] E. Kim, K. Kim, D. Son, J. Kim, S. Won, W.S. Hong, J. Sok, K. Park, Microelectron. Eng. 85 (2008) 2370.
[4] B. Gosh, H. Liu, B. Winstead, M.C. Foisy, S.K. Banerjee, Solid State Electron. 54 (2010) 1295.
[5] V. Cocheteau, P. Mur, T. Billon, E. Scheid, B. Caussat, Appl. Surf. Sci. 254 (2008) 2927.
[6] F. Mazen, T. Baron, G. Brémond, N. Buffet, N. Rochat, P. Mur, M.N. Séméria, J. Electrochem. Soc. 150 (2003) G203.
[7] G. Nicotra, R.A. Puglisi, S. Lombardo, C. Spinella, M. Vulpio, G. Ammendola, M. Bileci, C. Gerardi, J. Appl. Phys. 95 (2004) 2049.
[8] D. Din, I. Perez-Wurfl, G. Conibeer, M.A. Green, Sol. Energy Mater. Sol. Cells 94 (2010) 2238.
[9] L.V. Mercaldo, P. Delli Veneri, E. Esposito, E. Massera, I. Usatii, C. Privato, Mater. Sci. Eng. B 159–160 (2009) 74.
[10] W.T. Leach, J. Zhu, J.G. Ekerdt, J. Cryst. Growth 243 (2002) 30.
[11] Y. Kajikawa, S. Noda, Appl. Surf. Sci. 245 (2004) 281.
[12] G. Nicotra, S. Lomabardo, C. Spinella, G. Ammendola, C. Gerardi, C. Demuro, Appl. Surf. Sci. 205 (2003) 304.
[13] M.E. Coltrin, R.J. Kee, G.H. Evans, J. Electrochem. Soc. 136 (1989) 819.
[14] P. Ho, M.E. Coltrin, W.G. Breiland, J. Phys. Chem. 98 (1994) 10138.
[15] C.R. Kleijn, J. Electrochem. Soc. 138 (1991) 2190.
[16] Y.B. Wang, F. Teyssandier, J. Simon, R. Feurer, J. Electrochem. Soc. 141 (1994) 824.
[17] C. Cordier, E. Dehan, E. Scheid, P. Duverneuil, Mater. Sci. Eng. B 37 (1996) 30.
[18] E.F. Vansant, P. Van der Voort, K.C. Vrancken, Stud. Surf. Sci. Catal. (1995) 93.
[19] S. Miyazaki, Y. Hamamoto, E. Yoshida, M. Ikeda, M. Hirose, Thin Solid Films 369 (2000) 55.
[20] F. Mazen, Ph.D thesis INSA, Lyon, France, 2003.
[21] C.R. Kleijn, Thin Solid Films 365 (2000) 294.
[22] A.M. Rinaldi, S. Carrà, M. Rampoldi, M.C. Martignoni, M. Masi, J. Phys. IV Pr8 (1999) 189.
[23] D. Cai, L.L. Zheng, Y. Wan, A.V. Hariharan, M. Chandra, J. Cryst. Growth 250 (2003) 41.
[24] V. Cocheteau, P. Mur, T. Billon, E. Scheid, B. Caussat, Chem. Eng. J. 140 (2008) 600.
[25] I. Zahi, PhD thesis, INP Toulouse, France (2009).
[26] T.E. Wilke, K.A. Turner, C.G. Takoudis, Chem. Eng. Sci. 41 (1986) 643.
[27] I. Zahi, A. Estève, M. Djafari Rouhani, B. Caussat, H. Vergnes, P. Mur, Ph. Blaise, E. Scheid, Surf. Coat. Technol. 201 (2007) 8854.
[28] J.H. De Boer, M.E. Hermans, J. Vleeskens, Koninkl. Ned. Acad. Wetenschap. B 60 (1957) 45.
[29] J.B. Peri, A.L. Hensley, J. Phys. Chem. 72 (1968) 2926.
[30] L.T. Zhuravlev, Colloids Surf. A: Physicochem. Eng. Asp. 173 (2000) 1.
[31] R.B. Bird, W.E. Stewart, E.N. Lightfoot, Transp. Phenom. Wiley International Edition, New-York, 1960.
[32] M.T. Swihart, S.L. Girshick, J. Phys. Chem. B 103 (1999) 64.
[33] C. Cavallotti, A. Barbato, A. Veneroni, J. Cryst. Growth 266 (2004) 371.